Environmental Science & Technology

pubs.acs.org/est

Article

Aromatic Photo-oxidation, A New Source of Atmospheric Acidity

Sainan Wang,* Mike J. Newland, Wei Deng, Andrew R. Rickard, Jacqueline F. Hamilton, Amalia Muñoz, Milagros Ródenas, Monica M. Vázquez, Liming Wang, and Xinming Wang*

Cite This: *Environ. Sci. Technol.* 2020, 54, 7798−7806

Read Online

ACCESS | Metrics & More | Article Recommendations | Supporting Information

ABSTRACT: Formic acid (HCOOH), one of the most important and ubiquitous organic acids in the Earth's atmosphere, contributes substantially to atmospheric acidity and affects pH-dependent reactions in the aqueous phase. However, based on the current mechanistic understanding, even the most advanced chemical models significantly underestimate the HCOOH concentrations when compared to ambient observations at both ground-level and high altitude, thus underrating its atmospheric impact. Here we reveal new chemical pathways to HCOOH formation from reactions of both O_3 and OH with ketene-enols, which are important and to date undiscovered intermediates produced in the photo-oxidation of aromatics and furans. We highlight that the estimated yields of HCOOH from ketene-enol oxidation are up to 60% in polluted urban areas and greater than 30% even in the continental background. Our theoretical calculations are further supported by a chamber experiment evaluation. Considering that aromatic compounds are highly reactive and contribute ca. 10% to global nonmethane hydrocarbon emissions and 20% in urban areas, the new oxidation pathways presented here should help to narrow the budget gap of HCOOH and other small organic acids and can be relevant in any environment with high aromatic emissions, including urban areas and biomass burning plumes.

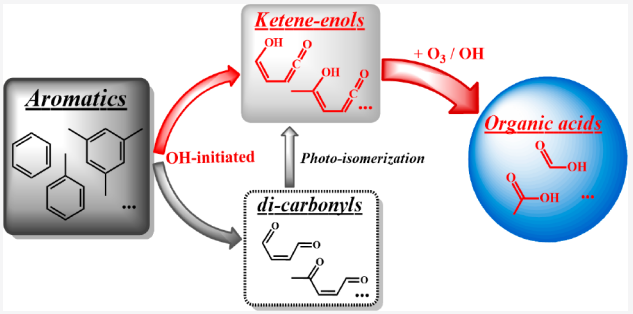

INTRODUCTION

Formic acid (HCOOH) is one of the most abundant and ubiquitous acids in earth's atmosphere, with a significant influence on precipitation acidity, pH-dependent aqueous-phase reactions, and in-cloud OH chemistry.[1] HCOOH can also play a role in forming cloud condensation nuclei (CCN),[2] indirectly influencing radiative forcing and hence climate. Sources of HCOOH include direct emission from terrestrial vegetation and vehicle exhaust and secondary formation from photochemical oxidation of volatile organic compounds (VOCs), in particular, biogenic species such as isoprene and terpenoids.[3] Recent work has also indicated that biomass burning is an important source of HCOOH.[4]

Both ground-based and airborne/satellite observations of HCOOH concentrations in the atmosphere are substantially under-predicted by current models, at times by a factor of 4 or more,[3,5] implying that there are large missing sources. A number of potential secondary atmospheric sources have been identified, including OH oxidation of enols,[6] OH oxidation of secondary products of isoprene oxidation such as α-hydroxy carbonyls[7] and isoprene nitrates,[8] and reaction of the Criegee intermediate CH_2OO with water vapor.[9] However, even when all of these sources are incorporated into atmospheric models, a large gap remains in the HCOOH budget, with observations 2−3 times larger than model predictions.[10] These sources also cannot explain the large and rapid secondary photochemical formation of HCOOH observed in urban areas dominated by anthropogenic activities, in fire plumes, or in oil- and gas-producing areas.[4,5,11,12]

Yuan et al. showed that the modeled HCOOH concentration in the wintertime at a site in the Uintah Basin (Utah), an oil- and gas-producing region with large emissions of aromatic hydrocarbons, high photochemical reactivity, and weak biogenic influences, was greatly improved by incorporating a source from aromatics to the model but was little affected by other modified cases.[12] HCOOH formation has also been reported in chamber experiments of the oxidation of aromatics, with yields up to 6−13% for various aromatic precursors and reaction conditions.[13−16] Although it is known that HCOOH can be released from illuminated chamber walls, the observed production cannot be explained solely by this process. Therefore, although both experimental evidence and chemical box model simulations indicate that the oxidation of aromatic species might produce HCOOH, the formation mechanisms and yields are still open questions.

Aromatic hydrocarbons are ubiquitous in the atmosphere, with anthropogenic emissions from vehicle exhaust and solvent

Received: January 28, 2020
Revised: May 7, 2020
Accepted: June 1, 2020
Published: June 1, 2020

https://dx.doi.org/10.1021/acs.est.0c00526
Environ. Sci. Technol. 2020, 54, 7798−7806

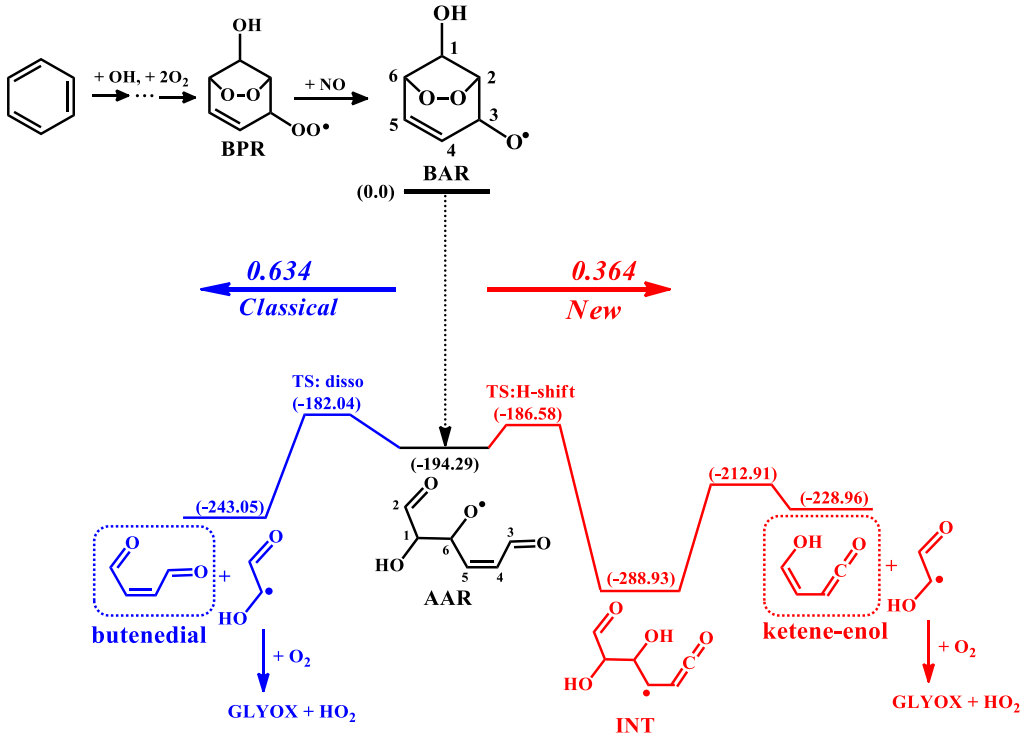

Figure 1. Schematic potential energy profiles for two different reactions of aliphatic alkoxy radical (AAR) at the level of ROCBS-QB3 (ΔE_{0K}, in kilojoules per mole). Classical decomposition to butenedial is marked in blue, and the new proposed H-shift isomerization and further decomposition to ketene-enol are in red.

evaporations and natural sources such as biomass burning and vegetation. While the oxidation of aromatics has been examined in a large number of studies,[15,17−20] significant uncertainties still exist in the general degradation chemical mechanisms and constraining the carbon balance.

It is well-established that the oxidation of aromatic compounds is initiated by reaction with OH radicals via H-abstraction from the alkyl groups or OH-addition to the aromatic ring, followed by further reactions to form peroxide bicyclic peroxy radicals (**BPRs**) (Figure 1).[21−24] In the presence of NO, a **BPR** is mainly transformed into the corresponding peroxide bicyclic alkoxy radical (**BAR**) which undergoes ring-opening that is presumed to lead to equal amounts of α-dicarbonyl and unsaturated 1,4-dicarbonyl coproducts.[25] However, experimentally determined α-dicarbonyl yields consistently exceed that of unsaturated 1,4-dicarbonyls.[20,26,27] This may be due to difficulties in measuring unsaturated 1,4-dicarbonyl species owing to their high reactivity. Alternatively, it may suggest that our current understanding of the ring-opening mechanism, and its subsequent chemistry, is incomplete. In addition to the OH oxidation of the benzene ring aromatics such as benzene, toluene, and xylenes, unsaturated 1,4-dicarbonyls are also formed as major ring-opening products in the atmospheric oxidation of furans, which are emitted in significant amounts in biomass burning events.[28,29] The dominant fate of unsaturated 1,4-dicarbonyls in the atmosphere was recently shown in chamber studies to be photoisomerization to a ketene-enol,[30] which might account for the discrepancies in the yield between butenedial and glyoxal. However, the subsequent chemistry of these species is entirely unknown.

In this work, our theoretical calculations on the benzene system present a new reaction pathway following the ring-opening routes in **BAR** leading to the primary formation of a ketene-enol species and coproduct glyoxal. We further investigate subsequent oxidation of the ketene-enol with the major atmospheric oxidants O_3 and OH and find significant production of HCOOH from a number of pathways. The predicted mechanisms are further confirmed by a chamber experiment evaluation and modeling study. The results of this study suggest, for the first time, that the formation of HCOOH from the reactions of ketene-enols produced in the photo-oxidation of benzene, alkylbenzenes, and furans is an important secondary HCOOH source that is missing in current atmospheric models.

METHODS

Theoretical Methods. All the molecular structures were optimized at the DFT-M06-2X/6-311++G(2df, 2p) level, which has been assessed to be suitable for thermokinetic studies.[31] The optimized structures were submitted to electronic energies using the complete-basis-set model chemistry (CBS-QB3)[32] and the explicitly correlated CCSD-(T)-F12a (F12) method with cc-pVDZ-F12 or cc-pVTZ-F12 basis set,[33] all using the restricted open-shell wave functions for the radical species. The F12 calculations were performed by using the Molpro 2015 package,[34] and the rest were carried out using the *Gaussian 09* suite of programs.[35]

The reaction rate coefficients of the unimolecular reactions were calculated using the unimolecular rate theory coupled with the energy-grained master equation for collisional energy transfer (RRKM-ME),[36] and the rate coefficients of bimolecular reactions were determined using traditional transition-state theory.[37] The RRKM-ME calculations were carried out using the Mesmer code.[38] A single exponential-down model was used to approximate the collisional energy

https://dx.doi.org/10.1021/acs.est.0c00526
Environ. Sci. Technol. 2020, 54, 7798−7806

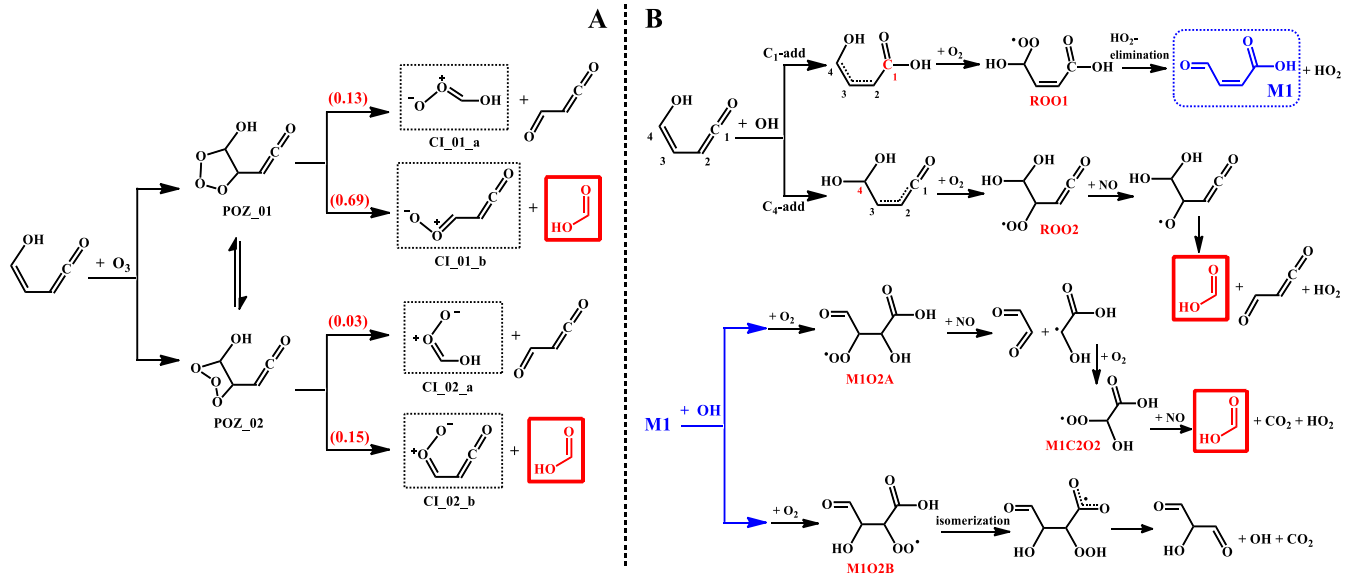

Figure 2. (A) Reaction scheme of ketene-enol with O_3. Two primary ozonides (POZ_01 and POZ_02) with differing orientations of the middle O atom can undergo rapid interconversion. Criegee intermediates (CI) are shown in their zwitterionic forms. The branching ratios of the four different pathways are shown in brackets. (B) Reaction scheme of OH additions to C_1 and C_4 position of ketene-enol. For C_4-addition to ketene-enol, the formed peroxy radical (ROO2) would react with $NO/HO_2/RO_2$ to form alkoxy radical, which then decomposes to formyl ketene and HCOOH. The peroxy radical ROO1 formed from C_1-addition would further undergo unimolecular HO_2 elimination to form 4-oxo-butenoic acid (M1), which can undergo secondary reaction with OH to produce HCOOH.

transfer with $\langle \Delta E \rangle_{down}$ of 250 cm^{-1}. The collisional parameters were estimated using the method of Gilbert and Smith,[39] and the asymmetric Eckart model was used for the tunneling correction factors.[40]

Chamber Experiment and Box Modeling. The experiment was performed on July 27, 2009, as part of the Toluene OXidation In a Chamber (TOXIC) campaign (July 2009), with initial mixing ratios of 125 ppbv of (*E*)-butenedial and 520 ppbv of NO. All VOC precursors and products shown, and HONO, were measured by FTIR. NO was measured by chemiluminescence.

Box model runs were performed with the AtChem2 model[41] using two different chemical mechanisms: (i) MCMv3.3.1, the butenedial mechanism extracted from the MCMv3.3.1 (mcm.york.ac.uk);[42] (ii) BASE, the MCMv3.3.1 mechanism adapted using the photochemistry of butenedial described in Newland et al. (2019)[30] and the chemistry of the ketene-enol described in this work (Table S1). The model was constrained to measured $j(NO_2)$, and a chamber-specific auxiliary mechanism is included for the EUPHORE chamber.[43]

RESULTS AND DISCUSSION

Primary Formation of the Ketene-enol in the Oxidation of Benzene. As shown in Figure 1, **BAR** would decompose through the breaking of the C_2-C_3 and the −O−O− bridge bonds, forming an aliphatic alkoxy radical (AAR) intermediate. We have identified the transition state of C_2-C_3 breakage and obtained an energy barrier of 33.4 kJ/mol at the ROCBS-QB3 level. Further breakage of the −O−O− bridge bond is barrierless.[44,45] Given the current mechanistic understanding, AAR would exclusively undergo decomposition, eventually forming butenedial accompanied by glyoxal (in blue in Figure 1).

However, here we present an unexpected 1,5 H-shift isomerization reaction in **AAR**, transferring an H atom from the carbonyl group $-C_{(3)}HO$ to the alkoxy radical with an energy barrier of 7.7 kJ/mol (as shown in red in Figure 1), being highly competitive with decomposition with an energy barrier of 12.2 kJ/mol. The 1,5 H-shift reaction is highly exothermic by −94.6 kJ/mol because of the formation of a resonance-stabilized intermediate species (**INT** in Figure 1) which greatly reduces the energy. Because of the substantial energy released from **BAR** to **AAR** (−194.29 kJ/mol) and from the H-shift in **AAR** (−94.6 kJ/mol), the energized ketene-like intermediate species **INT** would undergo unimolecular decomposition rather than reacting with O_2, even though the former is endothermic and with an energy barrier of 76.02 kJ/mol. Decomposition would lead to the formation of a ketene-enol accompanied by glyoxal (Figure 1).

To obtain the yields of butenedial and ketene-enol from the two different pathways available for **AAR**, we paid special attention to quantify the branching ratio of the 1,5 H-shift influenced by multiple conformers and carried out RRKM-ME calculations. The predicted branching ratios forming butenedial and ketene-enol are 0.634 and 0.364, respectively, with the yield of the O_2-adduct being almost negligible (Figure S1). Glyoxal is the coproduct of both classical and the newly proposed 1,5 H-shift pathways, which might also partially account for the discrepancies in the yield between butenedial and glyoxal under dark conditions and without further photolysis of butenedial.[19,20,27]

Newland et al. recently showed that butenedial can also undergo rapid photoisomerization to form a ketene-enol.[30] Therefore, the ketene-enol can be formed either directly from primary decomposition of **BAR** as presented here or from the further photochemistry of butenedial. Thus, the actual yield of ketene-enol from **BAR** should be higher than we predict theoretically (0.364). The ketene-enol is expected to be reactive under atmospheric conditions owing to the presence of the ketene and enol moieties; therefore, reactions with the major atmospheric oxidants O_3 and OH radicals may be important atmospheric loss processes.

https://dx.doi.org/10.1021/acs.est.0c00526
Environ. Sci. Technol. 2020, 54, 7798−7806

HCOOH Formation from Ketene-enol Reaction with O_3 and OH Radicals. The reaction of the ketene-enol with O_3 follows the Criegee mechanism,[46] i.e., O_3 adds to the unsaturated enol bond and forms two primary ozonides (denoted as POZ_01 and POZ_02 in Figure 2A), which contain excess energy to break the ring and eventually form four different Criegee intermediates (CIs). It is noted that the ketene double bond is not favored by the electrophilic O_3 addition because of the unique cumulene structure of ketene with substantial positive charge on the carbonyl carbon. We have obtained the potential energy surface at the RHF-CCSD(T)-F12a level with the basis set cc-pVTZ-F12. Using the traditional transition-state theory, the rate coefficients of O_3 additions forming POZ_01 and POZ_02 at 298 K are estimated as 1.21×10^{-15} and 2.36×10^{-16} cm^3 molecule^{-1} s^{-1}, respectively.

Each POZ undergoes two different ring scissions to form four Criegee intermediates, CI_01_a/b and CI_02_a/b, as shown in Figure 2A. Detailed energies are available in Table S1. Formyl ketene is formed as the coproduct of both CI_01_a and CI_02_a, and HCOOH is the coproduct of both CI_01_b and CI_02_b. Note that two POZs with differing orientations of the middle O atom can undergo rapid interconversion with a low barrier of < 15 kJ/mol. We have modeled the prompt formation of the four CIs using RRKM-ME calculations and set the formation processes of CIs as irreversible because of the substantial energy released. The calculation results show that the branching ratios of the formation of CI_01_a, CI_01_b, CI_02_a, and CI_02_b are 0.13, 0.69, 0.03 and 0.15, respectively. Thus, the total primary yield of HCOOH from O_3 reactions with ketene-enol is 0.84.

Subsequent reactions of the four different CIs were also investigated. CI_01_a would cyclize to dioxirane, and CI_02_a would isomerize to performic acid, which has been well studied in previous work.[47] CI_01_b would cyclize to a 3-membered dioxirane over a barrier of 40.3 kJ/mol, while CI_02_b would go through a barrierless 1,5-cyclization to a 5-membered dioxolene. Both cyclic compounds are expected to be highly unstable and break into fragments. Detailed energies and reaction pathways are available in Table S1 and Figure S2.

As for site-specific OH addition to dienes such as isoprene, the reaction of ketene-enol with OH radicals proceeds mainly as OH additions to the two terminal carbons of C_1 and C_4 as shown in Figure 2B. Reaction energies are obtained at the RHF-UCCSD(T)-F12a level with the basis set cc-pVTZ-F12, and the rate coefficient of OH additions to C_1- and C_4-positions at 298 K are estimated as 7.52×10^{-11} and 4.27×10^{-11} cm^3 molecule^{-1} s^{-1}, respectively. The transition states for both C_1 and C_4 additions are submerged under the reactants by 15.79 and 16.04 kJ/mol, respectively. The rate constant of OH addition to ketene-enol at C_1 position is 2∼5 times faster than the reported OH reaction with ketene (CH_2CO) under various temperatures and pressures.[48,49] Compared with previous studies on the OH addition to vinyl alcohol (ethenol, CH_2CHOH) at the α-carbon, the relative energy of the transition state of C_4-addition predicted here is 2.6 kJ/mol lower than that reported by So et al.[6] and 3.1 kJ/mol lower than recently reported by Lei et al.[50] The slightly lower energy of the transition states and faster reaction rates we obtained here might be explained by the resonance stabilization of the radical formed after addition of OH to ketene-enol, similar to that of conjugated dienes.[51]

Owing to the presence of an allylic group after C_1-addition, a pair of peroxy radicals would be formed from O_2 additions to C_2 and C_4 positions. However, O_2 addition to C_2 is fast reversible with a reverse rate of 5.0×10^8 s^{-1} and therefore was not considered. The peroxy radical **ROO1** formed from O_2 addition to C_4 would undergo unimolecular HO_2 elimination to form 4-oxo-butenoic acid (**M1**), which is denoted as MALDALCO2H in the MCM and assigned to be formed from butenedial oxidation. **M1** could further react rapidly with OH and form HCOOH, as shown in Figure 2B. For C_4-addition to ketene-enol, further O_2 addition can take place only at the C_3 position. The formed peroxy radical (**ROO2**) could react with $NO/HO_2/RO_2$ to form the alkoxy radical, which then would decompose to formyl ketene and HCOOH. Detailed reaction energies are available in Table S1.

Chamber Experiment and Mechanism Simulations. In order to assess the theoretical calculations presented, model simulations were carried out with the proposed ketene-enol chemistry (Table 1) and compared to observations from an

Table 1. Calculated Effective Rate Coefficients

reaction	k (cm^3 molecule^{-1} s^{-1})
Ketene-enol + O_3 → CI_01_a + formyl ketene	2.34×10^{-16}
Ketene-enol + O_3 → CI_01_b + HCOOH	1.24×10^{-15}
Ketene-enol + O_3 → CI_02_a + HCOOH	2.70×10^{-16}
Ketene-enol + O_3 → CI_02_b + formyl ketene	5.40×10^{-17}
Ketene-enol + OH (C_1-add) → M1 + HO_2	7.52×10^{-11}
Ketene-enol + OH (C_4-add) → HCOOH + formyl ketene + OH	4.27×10^{-11}

(*E*)-butenedial photo-oxidation experiment performed in the large outdoor environmental simulation chamber, EUPHORE.[52] The overall measured chemical production of HCOOH during the experiment was 10 ppbv (corrected for auxiliary chamber chemistry, see the Supporting Information), which gives an HCOOH yield of roughly 8% from (*E*)-butenedial under the conditions of the experiment.

A box model was used to compare the mechanisms presented herein (BASE, solid line) to the experimental measurements and to the Master Chemical Mechanism (MCMv3.3.1, dashed line).[42] More details and further model measurement comparisons are shown in the Supporting Information. As shown in Figure 3, the measured HCOOH (red diamonds) is well predicted by the BASE model run. The major HCOOH production channels in the experiment are shown in Figure S3. It should be noted that no chemical HCOOH production is present in the MCMv3.3.1 mechanism, and the production (dashed line in Figure 3) is exclusively from illumination of the chamber walls (Figure S4). Figure 4 shows the sensitivity of the modeled HCOOH production in the BASE run to the theoretically calculated rates of reaction of OH and O_3 with the ketene-enol. All rate constant adjustments are only a factor of 2, corresponding to the adjustment to the barrier of <2 kJ/mol at the room temperature, and thus within the expected uncertainties of the calculations at the RHF-CCSD(T)-F12a level with the basis set cc-pVTZ-F12. Doubling the rate of OH addition to C_1 (yellow dotted line) does not greatly increase HCOOH production, particularly early in the experiment because HCOOH is being formed as a second-generation product of the ketene-enol + OH reaction. Doubling the rate of OH addition to C_4 (blue dashed line), to 8.54×10^{-11} cm^3 s^{-1}, gives a good fit to the measured

https://dx.doi.org/10.1021/acs.est.0c00526
Environ. Sci. Technol. 2020, 54, 7798−7806

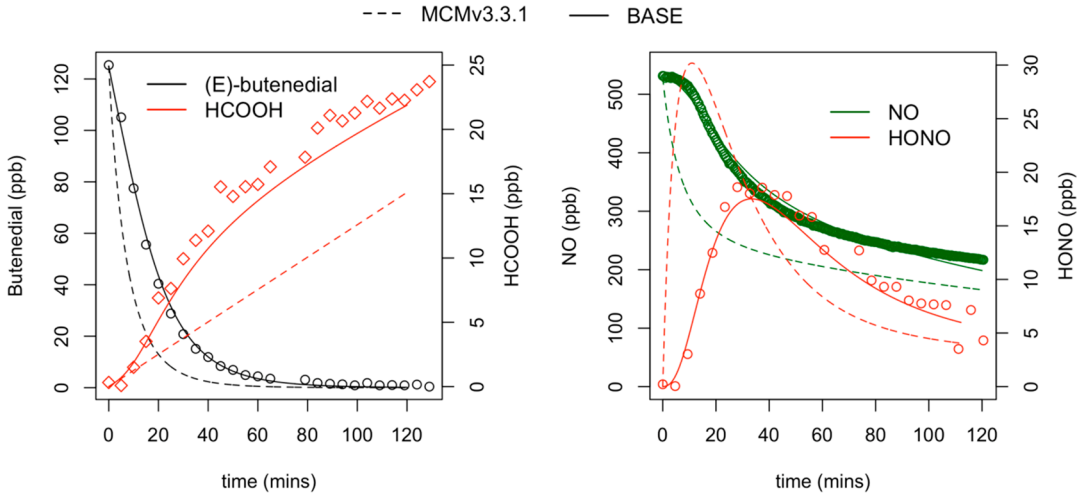

Figure 3. Chamber model versus measurement comparison of the EUPHORE (E)-butenedial photo-oxidation experiment (27/07/2009; chamber open at 15:13 local time). Butenedial (black circles), formic acid (red diamonds), NO (green circles), and HONO (red circles). Dashed lines are output from the MCMv3.3.1 model run (HCOOH wall source only); solid lines are from BASE model runs, using the chemistry presented here and in Newland et al. (2019).[30] The chamber is opened at time $t = 0$.

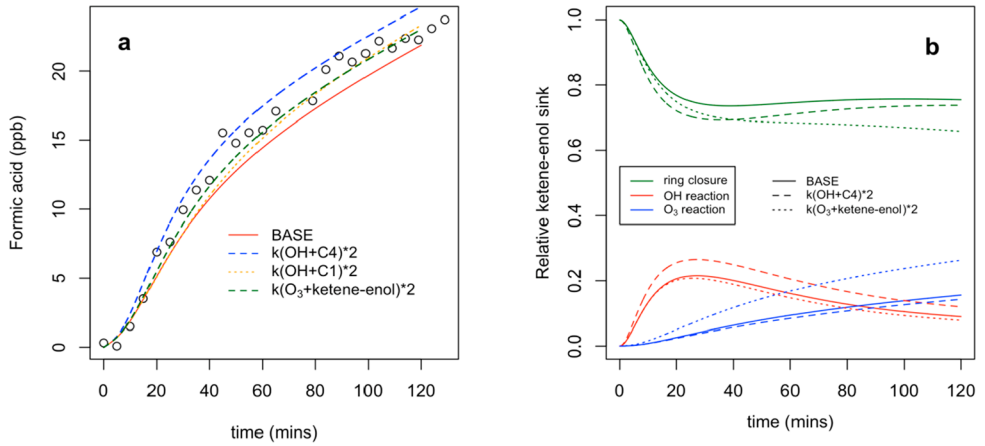

Figure 4. (a) Sensitivity of modeled HCOOH in BASE model run to the reaction rates of the ketene-enol with OH and O_3. (b) Relative sink of ketene-enol to ring closure and OH and O_3 reactions during experiment for three of the scenarios shown in panel a.

HCOOH. For the O_3 + ketene-enol reaction, doubling the calculated reaction rate (green dashed line) gives a good fit to the measurements.

The BASE run also fits the concentration−time profiles of most of the measured species better than the MCMv3.3.1 mechanism (Figure S5). Much of the improvement is driven by getting the timing and magnitude of the formation of the radicals OH and HO_2 right. In the MCMv3.3.1 run, NO is removed too quickly because of the production of large amounts of HO_2 in the mechanism. This reaction produces a large amount of OH which removes (*E*)-butenedial too fast and leads to the earlier formation of secondary products (Figure S5). However, Newland et al.[30] recently showed that photolysis of butenedial has low initial radical yields and the major channel is photoisomerization to the ketene-enol. It is also clear from comparison to the measured HONO (formed from OH + NO) and NO time-series that the MCMv3.3.1 run produces radicals too early, while the BASE run is in good agreement with the measurements.

Predicted HCOOH Production from the Photo-oxidation of Aromatics. Aromatic hydrocarbons including **BTEX** (benzene, toluene, ethylbenzene, and xylenes) are present at high concentrations in urban areas.[53,54] This work shows that OH oxidation of benzene will lead to the ketene-enol both directly via decomposition of the **BAR** following a 1,5 H-shift and from photoisomerization of the butenedial formed from classical decomposition of the **BAR** (under typical mid-day conditions ($j(NO_2) = 8 \times 10^{-3}$ s^{-1}; [OH] = 5×10^6 cm^{-3}), >75% of butenedial will photoisomerize to the ketene-enol). Ketene-enol species are also expected to be formed via both pathways in the photo-oxidation of more reactive monoaromatics, such as toluene, xylenes, and trimethylbenzenes. In the case of toluene, initiated OH addition and further O_2 additions would lead to multiple isomers of **BAR**. Subsequent reactions of selected **BAR** isomers are shown in Figure 5. We further calculated the branching ratio for classical decompositions and new proposed 1,5 H-shift reactions of different **BAR** isomers from toluene oxidation (Table S1). Combining with the proportion of different **BAR** isomers, we obtained the yield of dicarbonyls and ketene-enols as 0.38 and 0.13, respectively (Table S2). With the presence of a methyl group, ketene-enol oxidation can form both formic and acetic acid (Figure 5). Because of the diversity of **BAR**s formed in the photo-oxidation of alkyl

https://dx.doi.org/10.1021/acs.est.0c00526
Environ. Sci. Technol. 2020, 54, 7798−7806

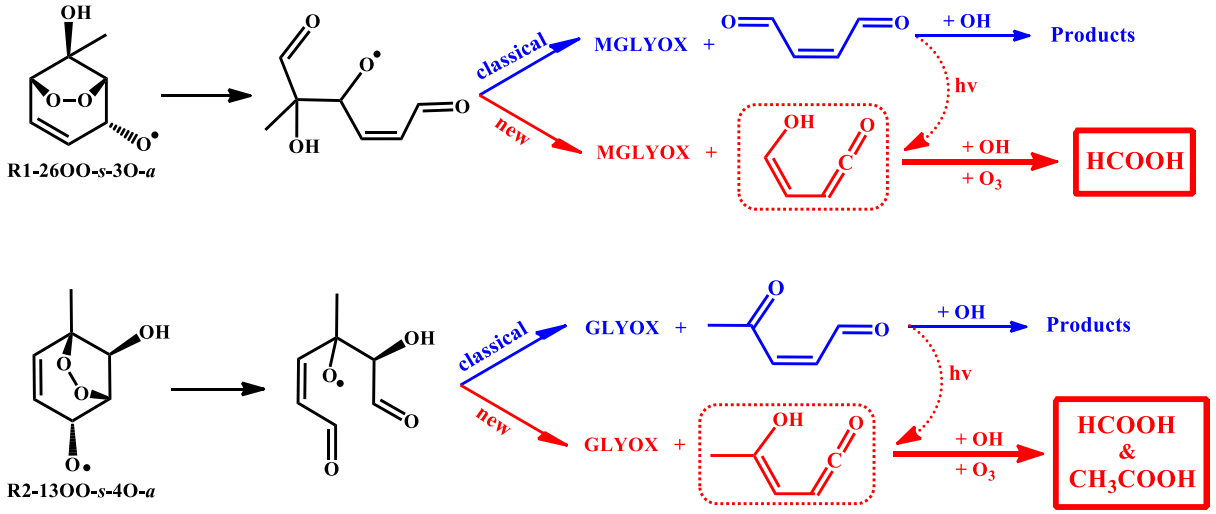

Figure 5. Direct formation pathways for formic (HCOOH) and acetic acid (CH_3COOH) from selected **BAR** isomers formed in the oxidation of toluene. **BAR**s are denoted as R*n*-*ij*OO-*s*-*k*O-*a*, in which *n* is the site of OH addition; *i* and *j* are the sites connecting the −OO− unit; *k* is the site of the second O_2 addition, and *a*/*s* is the *anti*/*syn* conformer, representing the direction of −OO− or −O relative to the −OH group. Two ketene-enol species formed directly from **BAR**s or from photoisomerization of unsaturated dicarbonyls are shown in the dashed boxes. Further oxidation of ketene-enols with OH/O_3 can form HCOOH and CH_3COOH.

Table 2. Loss Rates of Ketene-enol to Reaction with OH, O_3, and Ring Closure and HCOOH Yields (Assuming All RO_2 Reacts with NO), under a Set of Atmospherically Relevant Scenarios[a]

			relative fractional losses of ketene-enol[b]				HCOOH/CH_3COOH production (ppt hr^{-1})[d]		
scenario[c]	[OH] (cm^{-3})	[O_3] (ppbv)	L_{OH}	L_{O_3}	L_{RC}	HCOOH yield from ketene-enol	benzene	toluene	furan
polluted urban (summer)	1×10^7	150	0.11	0.61	0.29	0.59	7	70	372
polluted urban (winter)	5×10^6	100	0.07	0.54	0.39	0.51	3	31	179
continental background (summer)	4×10^6	50	0.08	0.38	0.54	0.38	2	19	118
continental background (winter)	2×10^6	35	0.05	0.31	0.64	0.30	1	7	49

[a]HCOOH/CH_3COOH production rate (ppt hr^{-1}) from a range of aromatic compounds in each scenario; summer and winter $j(NO_2) = 8 \times 10^{-3}$ s^{-1} and 6×10^{-3} s^{-1}, respectively; k(unsaturated 1,4 dicarbonyl + OH) = 5×10^{-11} molecules cm^{-3} s^{-1}. [b]L_{OH} = loss of ketene-enol to reaction with OH; L_{O_3} = loss to reaction with ozone; L_{RC} = loss to ring closure. [c]See e.g. Stone et al. (2012) for example OH concentrations, Parrish et al. (2012) for continental background ozone mixing ratios.[56,57] [d]Assuming an aromatic mixing ratio of 1 ppbv; **BAR** from benzene behaves as reported here, i.e. 0.364 decompose directly to the ketene-enol and 0.634 to the unsaturated 1,4 dicarbonyl; branching ratios of ketene-enols and unsaturated 1,4-dicarbonyls from different **BAR** isomers from toluene are shown in Table S2.

substituted aromatic compounds, and the ambiguous photolysis rate of specific alkyl-substituted unsaturated dicarbonyls to the corresponding ketene-enol, the yields of HCOOH and other small organic acids such as CH_3COOH need to be studied carefully in the future. Using the calculated rate coefficients for reactions of ketene-enol with O_3 and OH (Table 1) and the ring-closure rate coefficient of 3.2×10^{-3} s^{-1} reported recently,[30] we estimate the loss of ketene-enol to reactions with OH na dO_3 and to ring closure for a range of atmospherically relevant scenarios (Table 2). A possible photochemical sink for the ketene-enol is not thought to be important under tropospheric conditions, with Newland et al.[30] observing no change in the removal rate of the ketene-enol in the dark compared to the light. Recent studies from field observations and satellite retrievals have indicated severe ozone pollution in China where hourly maximum ozone concentrations frequently exceeded 150 ppbv.[55] For these high ozone scenarios, ketene-enol removal is dominated by reaction with O_3, and even under "background" conditions ozonolysis still accounts for ≥30% of the sink.

Oxidation of the ketene-enol then produces HCOOH, with the yield strongly dependent on the concentrations of O_3 and OH. The predicted HCOOH yield from ketene-enol reactions is ≥30% for all scenarios shown in Table 2 and >50% for polluted scenarios. The HCOOH/CH_3COOH production rates (ppt hr^{-1}) for OH-initiated oxidation of benzene, toluene, and furan for each scenario are calculated in Table 2, assuming a mixing ratio of the aromatic of 1 ppbv. On a per molecule basis the species with faster OH reaction rates have higher acid production rates. Toluene, as the dominant aromatic compound in urban environments, has a predicted production rate of HCOOH and CH_3COOH about 10 times faster than predicted for benzene. Furthermore, as furan has a predicted production rate of HCOOH even higher than toluene (Table 2), although mixing ratios of furans are low in the ambient atmosphere, they have been measured to be up to tens of ppb in biomass burning plumes[58] and hence have the potential to make a significant contribution to substantial secondary organic acid production in fire plumes.[4]

Atmospheric Implications. The mechanistic work presented here highlights a new and important role of ketene-enols, formed from the OH-initiated oxidation of aromatic hydrocarbons and furans, in contributing to a significant missing source of atmospheric acidity through the

https://dx.doi.org/10.1021/acs.est.0c00526
Environ. Sci. Technol. 2020, 54, 7798−7806

formation of HCOOH and other small organic acids via bimolecular reaction with O_3 and OH radicals, and in narrowing the gap between observed and modeled HCOOH concentrations in urban areas and in biomass burning plumes. Nonetheless, further detailed experimental and theoretical work is required on the atmospheric chemistry of ketene-enols to confirm the mechanistic details of these pathways in the oxidation of other alkyl substituted and oxygenated aromatic hydrocarbons and to consider the influence of atmospheric conditions such as temperature and actinic flux.

■ ASSOCIATED CONTENT

Supporting Information

The Supporting Information is available free of charge at https://pubs.acs.org/doi/10.1021/acs.est.0c00526.

Details in chamber experiment and box modeling; calculated reaction energies and the kinetics results (Tables S1 and S2 and Figures S1 and S2); additional chemical mechanism used in BASE model run (Table S3); EUPHORE auxiliary mechanism (Table S4); major HCOOH production channels (Figure S3); formic acid and ozone wall production rates (Figure S4); model-measurement comparison of other species (Figure S5) (PDF)

■ AUTHOR INFORMATION

Corresponding Authors

Sainan Wang − *State Key Laboratory of Organic Geochemistry and Guangdong Key Laboratory of Environmental Protection and Resources Utilization, Guangzhou Institute of Geochemistry, Chinese Academy of Sciences, Guangzhou, China;* orcid.org/0000-0002-5759-1484; Email: wangsainan@gig.ac.cn

Xinming Wang − *State Key Laboratory of Organic Geochemistry and Guangdong Key Laboratory of Environmental Protection and Resources Utilization, Guangzhou Institute of Geochemistry, Chinese Academy of Sciences, Guangzhou, China;* orcid.org/0000-0002-1982-0928; Email: wangxm@gig.ac.cn

Authors

Mike J. Newland − *Wolfson Atmospheric Chemistry Laboratories, Department of Chemistry, University of York, York YO10 5DD, U.K.;* orcid.org/0000-0003-4529-3874

Wei Deng − *State Key Laboratory of Organic Geochemistry and Guangdong Key Laboratory of Environmental Protection and Resources Utilization, Guangzhou Institute of Geochemistry, Chinese Academy of Sciences, Guangzhou, China*

Andrew R. Rickard − *Wolfson Atmospheric Chemistry Laboratories, Department of Chemistry and National Centre for Atmospheric Science, Wolfson Atmospheric Chemistry Laboratories, University of York, York YO10 5DD, U.K.;* orcid.org/0000-0003-2203-3471

Jacqueline F. Hamilton − *Wolfson Atmospheric Chemistry Laboratories, Department of Chemistry, University of York, York YO10 5DD, U.K.*

Amalia Muñoz − *Fundación CEAM, EUPHORE Laboratories, Paterna, Valencia, Spain*

Milagros Ródenas − *Fundación CEAM, EUPHORE Laboratories, Paterna, Valencia, Spain*

Monica M. Vázquez − *Fundación CEAM, EUPHORE Laboratories, Paterna, Valencia, Spain*

Liming Wang − *School of Chemistry & Chemical Engineering, South China University of Technology, Guangzhou, China;* orcid.org/0000-0002-8953-250X

Complete contact information is available at: https://pubs.acs.org/10.1021/acs.est.0c00526

Notes

The authors declare no competing financial interest.

■ ACKNOWLEDGMENTS

This work was supported by the National Key Research and Development Program (2016YFC0202204), the Chinese Academy of Sciences (QYZDJ-SSW-DQC032), and Guangdong Science and Technology Department (2017BT01Z134 and 2016TQ03Z993). S.W. acknowledges support from the National Science Foundation for Young Scientists of China (41905116) and the China Postdoctoral Science Foundation (2019M660215). S.W. and L.W. acknowledge the financial support from the National Science Foundation the National Key Research and Development Program (2017YFC0212802) and NSF China (21677051). M.N., A.R.R., and J.F.H. acknowledge support from the Atmospheric Pollution and Human Health in a Chinese Megacity Impact Project NE/S006648/1. M.N., A.R.R., A.M., and M.R. acknowledge funding from the European Union's Horizon 2020 research and innovation programme through the EUROCHAMP-2020 Infrastructure Activity under Grant Agreement No. 730997. We acknowledge the assistance of scientists at EUPHORE and the TOXIC project, especially James Lee and Sarah Møller (University of York; NO_x measurements) and Bernard Golding (Newcastle University; butenedial synthesis). The TOXIC project was supported by a Trans-National Access Grant though the Eurochamp-2 programme (E2-2009-06-24-0001). EUPHORE chambers from Fundacion CEAM are partly supported by the IMAGINA-Prometeo project (PROMETEO2019/110) and by Generalitat Valenciana.

■ REFERENCES

(1) Khare, P.; Kumar, N.; Kumari, K. M.; Srivastava, S. S. Atmospheric formic and acetic acids: An overview. *Rev. Geophys.* **1999**, *37*, 227−248.

(2) Yu, S. Role of organic acids (formic, acetic, pyruvic and oxalic) in the formation of cloud condensation nuclei (CCN): a review. *Atmos. Res.* **2000**, *53*, 185−217.

(3) Paulot, F.; Wunch, D.; Crounse, J. D.; Toon, G. C.; Millet, D. B.; DeCarlo, P. F.; Vigouroux, C.; Deutscher, N. M.; González Abad, G.; Notholt, J.; Warneke, T.; Hannigan, J. W.; Warneke, C.; de Gouw, J. A.; Dunlea, E. J.; De Mazière, M.; Griffith, D. W. T.; Bernath, P.; Jimenez, J. L.; Wennberg, P. O. Importance of secondary sources in the atmospheric budgets of formic and acetic acids. *Atmos. Chem. Phys.* **2011**, *11*, 1989−2013.

(4) Chaliyakunnel, S.; Millet, D. B.; Wells, K. C.; Cady-Pereira, K. E.; Shephard, M. W. A Large Underestimate of Formic Acid from Tropical Fires: Constraints from Space-Borne Measurements. *Environ. Sci. Technol.* **2016**, *50*, 5631−5640.

(5) Le Breton, M.; McGillen, M. R.; Muller, J. B. A.; Bacak, A.; Shallcross, D. E.; Xiao, P.; Huey, L. G.; Tanner, D.; Coe, H.; Percival, C. J. Airborne observations of formic acid using a chemical ionization mass spectrometer. *Atmos. Meas. Tech.* **2012**, *5*, 3029−3039.

(6) So, S.; Wille, U.; da Silva, G. Atmospheric chemistry of enols: a theoretical study of the vinyl alcohol + OH + O(2) reaction mechanism. *Environ. Sci. Technol.* **2014**, *48*, 6694−6701.

(7) Butkovskaya, N. I.; Pouvesle, N.; Kukui, A.; Bras, G. L. Mechanism of the OH-initiated oxidation of glycolaldehyde over the

temperature range 233−296 K. *J. Phys. Chem. A* **2006**, *110*, 13492−13499.
(8) Paulot, F.; Crounse, J. D.; Kjaergaard, H. G.; Kroll, J. H.; Seinfeld, J. H.; Wennberg, P. O. Isoprene photooxidation: new insights into the production of acids and organic nitrates. *Atmos. Chem. Phys.* **2009**, *9*, 1479−1501.
(9) Francisco, J. S.; Eisfeld, W. Atmospheric oxidation mechanism of hydroxymethyl hydroperoxide†. *J. Phys. Chem. A* **2009**, *113*, 7593−7600.
(10) Millet, D. B.; Baasandorj, M.; Farmer, D. K.; Thornton, J. A.; Baumann, K.; Brophy, P.; Chaliyakunnel, S.; de Gouw, J. A.; Graus, M.; Hu, L.; Koss, A.; Lee, B. H.; Lopez-Hilfiker, F. D.; Neuman, J. A.; Paulot, F.; Peischl, J.; Pollack, I. B.; Ryerson, T. B.; Warneke, C.; Williams, B. J.; Xu, J. A large and ubiquitous source of atmospheric formic acid. *Atmos. Chem. Phys.* **2015**, *15*, 6283−6304.
(11) Veres, P. R.; Roberts, J. M.; Cochran, A. K.; Gilman, J. B.; Kuster, W. C.; Holloway, J. S.; Graus, M.; Flynn, J.; Lefer, B.; Warneke, C.; de Gouw, J. Evidence of rapid production of organic acids in an urban air mass. *Geophys. Res. Lett.* **2011**, *38*, L17807.
(12) Yuan, B.; Veres, P. R.; Warneke, C.; Roberts, J. M.; Gilman, J. B.; Koss, A.; Edwards, P. M.; Graus, M.; Kuster, W. C.; Li, S. M.; Wild, R. J.; Brown, S. S.; Dubé, W. P.; Lerner, B. M.; Williams, E. J.; Johnson, J. E.; Quinn, P. K.; Bates, T. S.; Lefer, B.; Hayes, P. L.; Jimenez, J. L.; Weber, R. J.; Zamora, R.; Ervens, B.; Millet, D. B.; Rappenglück, B.; de Gouw, J. A. Investigation of secondary formation of formic acid: urban environment vs. oil and gas producing region. *Atmos. Chem. Phys.* **2015**, *15*, 1975−1993.
(13) Wyche, K. P.; Monks, P. S.; Ellis, A. M.; Cordell, R. L.; Parker, A. E.; Whyte, C.; Metzger, A.; Dommen, J.; Duplissy, J.; Prevot, A. S. H.; Baltensperger, U.; Rickard, A. R.; Wulfert, F. Gas phase precursors to anthropogenic secondary organic aerosol: detailed observations of 1,3,5-trimethylbenzene photooxidation. *Atmos. Chem. Phys.* **2009**, *9*, 635−665.
(14) Borrás, E.; Tortajada-Genaro, L. A. Secondary organic aerosol formation from the photo-oxidation of benzene. *Atmos. Environ.* **2012**, *47*, 154−163.
(15) Berndt, T.; Boge, O. Gas-phase reaction of OH radicals with benzene: products and mechanism. *Phys. Chem. Chem. Phys.* **2001**, *3*, 4946−4956.
(16) Baltensperger, U.; Kalberer, M.; Dommen, J.; Paulsen, D.; Alfarra, M. R.; Coe, H.; Fisseha, R.; Gascho, A.; Gysel, M.; Nyeki, S.; Sax, M.; Steinbacher, M.; Prevot, A. S.; Sjogren, S.; Weingartner, E.; Zenobi, R. Secondary organic aerosols from anthropogenic and biogenic precursors. *Faraday Discuss.* **2005**, *130*, 265−278.
(17) Yu, J.; Jeffries, H. E.; Sexton, K. G. Atmospheric photooxidation of alkylbenzenes—I. Carbonyl product analyses. *Atmos. Environ.* **1997**, *31*, 2261−2280.
(18) Klotz, B.; Volkamer, R.; Hurley, M. D.; Andersen, M. P. S.; Nielsen, O. J.; Barnes, I.; Imamura, T.; Wirtz, K.; Becker, K.-H.; Platt, U.; Wallington, T. J.; Washida, N. OH-initiated oxidation of benzene: Part II. Influence of elevated NOx concentrations. *Phys. Chem. Chem. Phys.* **2002**, *4*, 4399−4411.
(19) Gomez Alvarez, E.; Viidanoja, J.; Munoz, A.; Wirtz, K.; Hjorth, J. Experimental confirmation of the dicarbonyl route in the photooxidation of toluene and benzene. *Environ. Sci. Technol.* **2007**, *41*, 8362−8369.
(20) Arey, J.; Obermeyer, G.; Aschmann, S. M.; Chattopadhyay, S.; Cusick, R. D.; Atkinson, R. Dicarbonyl products of the OH radical-initiated reaction of a series of aromatic hydrocarbons. *Environ. Sci. Technol.* **2009**, *43*, 683−689.
(21) Calvert, J. G. A. R.; Becker, K. H.; Kamens, R. M.; Seinfeld, J. H.; Wallington, T. J.; Yarwood, G. *The Mechanisms of Atmospheric Oxidation of the Aromatic Hydrocarbons*; Oxford University Press, 2002.
(22) Glowacki, D. R.; Wang, L.; Pilling, M. J. Evidence of formation of bicyclic species in the early stages of atmospheric benzene oxidation. *J. Phys. Chem. A* **2009**, *113*, 5385−5396.
(23) Birdsall, A. W.; Andreoni, J. F.; Elrod, M. J. Investigation of the role of bicyclic peroxy radicals in the oxidation mechanism of toluene. *J. Phys. Chem. A* **2010**, *114*, 10655−10663.
(24) Wu, R.; Pan, S.; Li, Y.; Wang, L. Atmospheric oxidation mechanism of toluene. *J. Phys. Chem. A* **2014**, *118*, 4533−4547.
(25) Aschmann, S. M.; Nishino, N.; Arey, J.; Atkinson, R. Products of the OH radical-initiated reactions of furan, 2- and 3-methylfuran, and 2,3- and 2,5-dimethylfuran in the presence of NO. *J. Phys. Chem. A* **2014**, *118*, 457−466.
(26) Volkamer, R.; Platt, U.; Wirtz, K. Primary and Secondary Glyoxal Formation from Aromatics: Experimental Evidence for the Bicycloalkyl−Radical Pathway from Benzene, Toluene, andp-Xylene. *J. Phys. Chem. A* **2001**, *105*, 7865−7874.
(27) Berndt, T.; Boge, O. Formation of phenol and carbonyls from the atmospheric reaction of OH radicals with benzene. *Phys. Chem. Chem. Phys.* **2006**, *8*, 1205−1214.
(28) Coggon, M. M.; Lim, C. Y.; Koss, A. R.; Sekimoto, K.; Yuan, B.; Gilman, J. B.; Hagan, D. H.; Selimovic, V.; Zarzana, K.; Brown, S. S.; Roberts, J. M.; Müller, M.; Yokelson, R.; Wisthaler, A.; Krechmer, J. E.; Jimenez, J. L.; Cappa, C.; Kroll, J.; de Gouw, J.; Warneke, C. OH-chemistry of non-methane organic gases (NMOG) emitted from laboratory and ambient biomass burning smoke: evaluating the influence of furans and oxygenated aromatics on ozone and secondary NMOG formation. *Atmos. Chem. Phys.* **2019**, *19*, 14875−14899.
(29) Yuan, Y.; Zhao, X.; Wang, S.; Wang, L. Atmospheric Oxidation of Furan and Methyl-Substituted Furans Initiated by Hydroxyl Radicals. *J. Phys. Chem. A* **2017**, *121*, 9306−9319.
(30) Newland, M. J.; Rea, G. J.; Thuner, L. P.; Henderson, A. P.; Golding, B. T.; Rickard, A. R.; Barnes, I.; Wenger, J. Photochemistry of 2-butenedial and 4-oxo-2-pentenal under atmospheric boundary layer conditions. *Phys. Chem. Chem. Phys.* **2019**, *21*, 1160−1171.
(31) Zhao, Y.; Truhlar, D. G. The M06 suite of density functionals for main group thermochemistry, thermochemical kinetics, noncovalent interactions, excited states, and transition elements: two new functionals and systematic testing of four M06-class functionals and 12 other functionals. *Theor. Chem. Acc.* **2008**, *120*, 215−241.
(32) Wood, G. P.; Radom, L.; Petersson, G. A.; Barnes, E. C.; Frisch, M. J.; Montgomery, J. A., Jr. A restricted-open-shell complete-basis-set model chemistry. *J. Chem. Phys.* **2006**, *125*, No. 094106.
(33) Adler, T. B.; Knizia, G.; Werner, H. J. A simple and efficient CCSD(T)-F12 approximation. *J. Chem. Phys.* **2007**, *127*, 221106.
(34) Werner, H. J. K. P. J.; Knizia, G.; Manby, F. R.; Schütz, M. C. P.; Györffy, W.; Kats, D.; Korona, T.; Lindh, R.; Mitrushenkov, A. R. R.; Shamasundar, K. R.; Adler, T. B.; Amos, R. D. B. A.; Berning, A.; Cooper, D. L.; Deegan, M. J. O.; Dobbyn, A. J. E. F.; Goll, E.; Hampel, C.; Hesselmann, A.; Hetzer, G. H. T.; Jansen, G.; Köppl, C.; Liu, Y.; Lloyd, A. W.; Mata, R. A. M. A. J.; McNicholas, S. J.; Meyer, W.; Mura, M. E.; Nicklass, A. O. N. D. P.; Palmieri, P.; Peng, D.; Pflüger, K.; Pitzer, R. R. M.; Shiozaki, T.; Stoll, H.; Stone, A. J.; Tarroni, R.; Thorsteinsson, T. W. M. *MOLPRO*, version 2015.1; MOLPRO: Stuttgart, Germany, 2015.
(35) Frisch, M. J.; Trucks, G. W.; Schlegel, H. B.; Scuseria, G. E.; Robb, M. A.; Cheeseman, J. R.; Scalmani, G.; Barone, V.; Mennucci, B.; Petersson, G. A.; Nakatsuji, H.; Caricato, M.; Li, X.; Hratchian, H. P.; Izmaylov, A. F.; Bloino, J.; Zheng, G.; Sonnenberg, J. L.; Hada, M.; Ehara, M.; Toyota, K.; Fukuda, R.; Hasegawa, J.; Ishida, M.; Nakajima, T.; Honda, Y.; Kitao, O.; Nakai, H.; Vreven, T.; Montgomery, J. A., Jr.; Peralta, J. E.; Ogliaro, F.; Bearpark, M.; Heyd, J. J.; Brothers, E.; Kudin, K. N.; Staroverov, V. N.; Kobayashi, R.; Normand, J.; Raghavachari, K.; Rendell, A.; Burant, J. C.; Iyengar, S. S.; Tomasi, J.; Cossi, M.; Rega, N.; Millam, J. M.; Klene, M.; Knox, J. E.; Cross, J. B.; Bakken, V.; Adamo, C.; Jaramillo, J.; Gomperts, R.; Stratmann, R. E.; Yazyev, O.; Austin, A. J.; Cammi, R.; Pomelli, C.; Ochterski, J. W.; Martin, R. L.; Morokuma, K.; Zakrzewski, V. G.; Voth, G. A.; Salvador, P.; Dannenberg, J. J.; Dapprich, S.; Daniels, A. D.; Farkas, O.; Foresman, J. B.; Ortiz, J. V.; Cioslowski, J.; Fox, D. J. *Gaussian 09*, revision A.01; Gaussian, Inc.: Wallingford, CT, 2009.
(36) Holbrook, K. A. P.; Robertson, S. H.; Robinson, P. J. *Unimolecular Reactions*, 2nd ed.; Wiley: New York, 1996.

https://dx.doi.org/10.1021/acs.est.0c00526
Environ. Sci. Technol. 2020, 54, 7798−7806

(37) Pilling, M. J.; Seakins, P. W. *Reaction Kinetics*; Oxford University Press Inc.: New York, 1999.
(38) Glowacki, D. R.; Liang, C. H.; Morley, C.; Pilling, M. J.; Robertson, S. H. MESMER: an open-source master equation solver for multi-energy well reactions. *J. Phys. Chem. A* **2012**, *116*, 9545−9560.
(39) Gilbert, R. G.; Smith, S. C. *Theory of Unimolecular and Recombination Reactions*; Blackwell Scientific Publications: Boston, 1990.
(40) Miller, W. H. Tunneling corrections to unimolecular rate constants, with application to formaldehyde. *J. Am. Chem. Soc.* **1979**, *101*, 6810−6814.
(41) Sommariva, R.; Cox, S.; Martin, C.; Borońska, K.; Young, J.; Jimack, P.; Pilling, M. J.; Matthaios, V. N.; Newland, M. J.; Panagi, M.; Bloss, W. J.; Monks, P. S.; Rickard, A. R. AtChem, an open source box-model for the Master Chemical Mechanism. *Geosci. Model Dev.* **2020**, *2019*, 1−27.
(42) Jenkin, M. E.; Young, J. C.; Rickard, A. R. The MCM v3.3.1 degradation scheme for isoprene. *Atmos. Chem. Phys.* **2015**, *15*, 11433−11459.
(43) Bloss, C.; Wagner, V.; Bonzanini, A.; Jenkin, M. E.; Wirtz, K.; Martin-Reviejo, M.; Pilling, M. J. Evaluation of detailed aromatic mechanisms (MCMv3 and MCMv3.1) against environmental chamber data. *Atmos. Chem. Phys.* **2005**, *5*, 623−639.
(44) Suh, I.; Zhao, J.; Zhang, R. Y. Unimolecular decomposition of aromatic bicyclic alkoxy radicals and their acyclic radicals. *Chem. Phys. Lett.* **2006**, *432*, 313−320.
(45) Wang, L.; Wu, R.; Xu, C. Atmospheric oxidation mechanism of benzene. Fates of alkoxy radical intermediates and revised mechanism. *J. Phys. Chem. A* **2013**, *117*, 14163−14168.
(46) Johnson, D.; Marston, G. The gas-phase ozonolysis of unsaturated volatile organic compounds in the troposphere. *Chem. Soc. Rev.* **2008**, *37*, 699−716.
(47) Vereecken, L.; Novelli, A.; Taraborrelli, D. Unimolecular decay strongly limits the atmospheric impact of Criegee intermediates. *Phys. Chem. Chem. Phys.* **2017**, *19*, 31599−31612.
(48) Brown, A. C.; Canosa-Mas, C. E.; Parr, A. D.; Wayne, R. P. Temperature dependence of the rate of the reaction between the OH radical and ketene. *Chem. Phys. Lett.* **1989**, *161*, 491−496.
(49) Oehlers, C.; Temps, F.; Wagner, H. G.; Wolf, M. Kinetics of the reaction of OH radicals with CH_2CO. *Berichte der Bunsengesellschaft für physikalische Chemie* **1992**, *96*, 171−175.
(50) Lei, X.; Wang, W.; Cai, J.; Wang, C.; Liu, F.; Wang, W. Atmospheric chemistry of enols: vinyl alcohol + OH + O_2 reaction revisited. *J. Phys. Chem. A* **2019**, *123*, 3205−3213.
(51) Peeters, J.; Boullart, W.; Pultau, V.; Vandenberk, S.; Vereecken, L. Structure-activity relationship for the addition of OH to (poly)alkenes: site-specific and total rate constants. *J. Phys. Chem. A* **2007**, *111*, 1618−1631.
(52) Munoz, A.; Vera, T.; Sidebottom, H.; Mellouki, A.; Borras, E.; Rodenas, M.; Clemente, E.; Vazquez, M. Studies on the atmospheric degradation of chlorpyrifos-methyl. *Environ. Sci. Technol.* **2011**, *45*, 1880−1886.
(53) Zhang, Y.; Mu, Y.; Meng, F.; Li, H.; Wang, X.; Zhang, W.; Mellouki, A.; Gao, J.; Zhang, X.; Wang, S.; Chai, F. The pollution levels of BTEX and carbonyls under haze and non-haze days in Beijing, China. *Sci. Total Environ.* **2014**, *490*, 391−396.
(54) Jia, C.; Batterman, S.; Godwin, C. VOCs in industrial, urban and suburban neighborhoods, Part 1: Indoor and outdoor concentrations, variation, and risk drivers. *Atmos. Environ.* **2008**, *42*, 2083−2100.
(55) Lu, X.; Hong, J.; Zhang, L.; Cooper, O. R.; Schultz, M. G.; Xu, X.; Wang, T.; Gao, M.; Zhao, Y.; Zhang, Y. Severe surface ozone pollution in China: a global perspective. *Environ. Sci. Technol. Lett.* **2018**, *5*, 487−494.
(56) Stone, D.; Whalley, L. K.; Heard, D. E. Tropospheric OH and HO2 radicals: field measurements and model comparisons. *Chem. Soc. Rev.* **2012**, *41*, 6348−6404.
(57) Parrish, D. D.; Law, K. S.; Staehelin, J.; Derwent, R.; Cooper, O. R.; Tanimoto, H.; Volz-Thomas, A.; Gilge, S.; Scheel, H. E.; Steinbacher, M.; Chan, E. Long-term changes in lower tropospheric baseline ozone concentrations at northern mid-latitudes. *Atmos. Chem. Phys.* **2012**, *12*, 11485−11504.
(58) Koss, A. R.; Sekimoto, K.; Gilman, J. B.; Selimovic, V.; Coggon, M. M.; Zarzana, K. J.; Yuan, B.; Lerner, B. M.; Brown, S. S.; Jimenez, J. L.; Krechmer, J.; Roberts, J. M.; Warneke, C.; Yokelson, R. J.; de Gouw, J. Non-methane organic gas emissions from biomass burning: identification, quantification, and emission factors from PTR-ToF during the FIREX 2016 laboratory experiment. *Atmos. Chem. Phys.* **2018**, *18*, 3299−3319.

https://dx.doi.org/10.1021/acs.est.0c00526
Environ. Sci. Technol. 2020, 54, 7798−7806